THE JOURNAL OF PHYSICAL CHEMISTRY C

ARTICLE

pubs.acs.org/JPCC

Enhanced Field Emission Performance of Ga-Doped $In_2O_3(ZnO)_3$ Superlattice Nanobelts

Lili Wu,[†,§] Quan Li,[†,§] Xitian Zhang,[*,†] Tianyou Zhai,[*,‡] Yoshio Bando,[‡] and Dmitri Golberg[‡]

[†]Heilongjiang Province Key Laboratory for Low-Dimensional Systems and Mesoscopic Physics, School of Physics and Electronic Engineering, Harbin Normal University, Harbin 150025, P. R. China

[‡]International Center for Young Scientists (ICYS) and International Center for Materials Nanoarchitectonics (MANA), National Institute for Materials Science (NIMS), Namiki 1-1, Tsukuba, Ibaraki 305-0044, Japan

[§]Department of Physics, The Chinese University of Hong Kong, Shatin, Hong Kong

ABSTRACT: Ga-doped $In_2O_3(ZnO)_3$ nanobelts were successfully fabricated via a simple chemical vapor deposition (CVD) process. The morphology, microstructure, and composition of the nanobelts were characterized by scanning electron microscopy, high resolution transmission electron microscopy, selected area electron diffraction, and X-ray photoelectron spectroscopy. The results confirm the formation of $In_2O_3(ZnO)_3$ superlattice nanobelts doped with Ga. The field-emission studies show a low turn-on electrical field, high field enhancement factor, and a good stability of the emission current. These results are valuable for the design, fabrication, and optimization of field emitters.

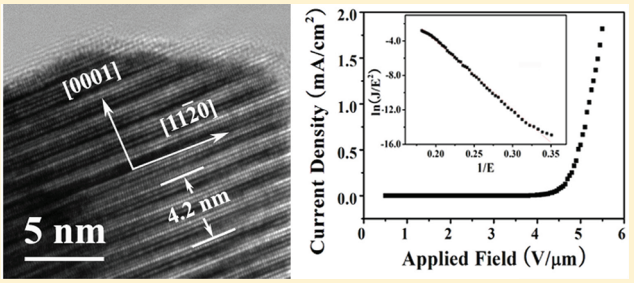

INTRODUCTION

One-dimensional (1D) nanostructures have stimulated great attention due to their promising applications in nanodevices. Field emission (FE), also called cold emission, is one of the main features of nanostructures based on the physical phenomenon of quantum tunneling, during which electrons are injected from a material surface into a vacuum under the influence of an applied electric field.[1,2] It is a more effective process than the normally employed thermionic emission because of its higher energy efficiency. In recent years, research on FE properties of 1D nanostructures has come to the forefront due to growing demand for displays, microwave amplifiers, and other vacuum microelectronic devices.[1,3,4] For these commercial applications, it is desirable to obtain a high current density at a small voltage drop between the anode and the cathode. Generally, there are two effective ways which can meet this challenge. One is optimizing the geometric factor by increasing the alignment or reducing the tip size of the nanostructures; the other is increasing conductivity and reducing the work function by selective element doping.[5−7]

Homologous compounds $In_2O_3(ZnO)_m$ (m = integer) have a superlattice structure and attract increasing attention due to promising applications for transparent conducting electrodes and high-temperature thermoelectric converters.[8−10] The fascinating crystal structure of $In_2O_3(ZnO)_m$ consists of InO_2^- layers (the In^{3+} ion is located at the octahedral site formed by oxygen) and $InO^+(ZnO)_m$ blocks (In^{3+} and Zn^{2+} ions take the trigonal-bipiramidal and tetrahedral coordinations, respectively) alternately stacked along the c-axis, forming a layered superlattice structure.[11,12] According to previous research, the carrier confinement effect of layered structure can decrease the effective surface barrier and then enhance FE current remarkably.[13−17] Besides, the good thermal stability of $In_2O_3(ZnO)_m$ at high temperatures could prevent $In_2O_3(ZnO)_m$ nanostructures from being deformed during the operations, which is a major challenge for a nanostructure emitter placed under large currents and high power density conditions. Thus, $In_2O_3(ZnO)_m$ should also be an ideal candidate for field emitters and is envisaged to exhibit excellent FE characteristics.[11,12]

1D $In_2O_3(ZnO)_m$ nanostructures have been synthesized by several groups.[11,18−25] However, the FE properties of $In_2O_3(ZnO)_m$ nanostructures have not been reported yet. Considering that the unique feature of $In_2O_3(ZnO)_m$, that is, the thickness of the $InO^+(ZnO)_m$ block, can be easily changed by varying the composition ratio of In_2O_3 and ZnO within the $In_2O_3(ZnO)_m$ structure (the value of m),[26] we can achieve easy control of the FE characteristics of 1D $In_2O_3(ZnO)_m$ nanostructures by controlling the m value. Fine m value tuning will change the thickness of the $InO^+(ZnO)_m$ block and enhance the FE current. On the other hand, we can implant selective elements into 1D $In_2O_3(ZnO)_m$ nanostructures to enhance their FE characteristics. It is well-known that group-III elements are efficient donors for II−VI group semiconductors. Many studies have already been performed regarding the synthesis and FE characteristics of group-III doped ZnO nanostructures.[5,27−30] Recently, Ga-, Al-, and Fe-doped $In_2O_3(ZnO)_m$ quaternary nanostructures have been synthesized.[10,31−33] Wang et al. reported the synthesis of $InGaO_3(ZnO)_m$ (m = 3, 5) nanowires and presented their

Received: August 4, 2011
Revised: September 30, 2011
Published: November 07, 2011

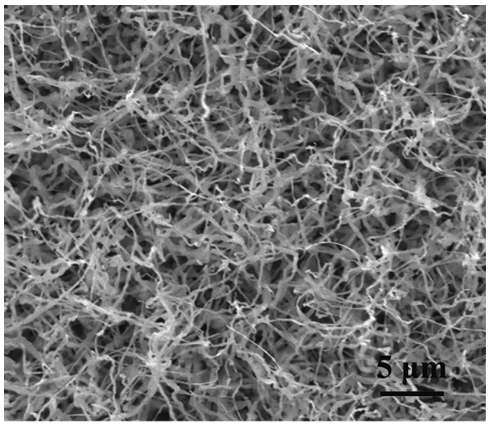

Figure 1. SEM image of Ga-doped $In_2O_3(ZnO)_3$ nanobelts showing the high quality of a product.

photoluminescence spectra.[31] Zhang et al. described the synthesis of $In_{2-x}Ga_xO_3(ZnO)_3$ nanobelts and $InAlO_3(ZnO)_m$ nanowires and elaborated a linear relationship between the periodicity and the diameter of $InAlO_3(ZnO)_m$ superlattice.[32,33] Yang et al. reported the synthesis of $InMO_3(ZnO)_m$ (M = Ga and Fe) nanowires and described the improved thermoelectric properties of $In_{2-x}Ga_xO_3(ZnO)_n$ nanowires.[10] In this paper, we designed and synthesized Ga-doped $In_2O_3(ZnO)_3$ nanobelts taking an advantage of the close bond lengths of Ga−O (1.92 Å) and In−O (2.1 Å). The FE properties of the Ga-doped $In_2O_3(ZnO)_3$ nanobelts were analyzed and discussed. These results should be valuable for the design, fabrication, and optimization of field emitters.

EXPERIMENTAL SECTION

The synthesis of Ga-doped $In_2O_3(ZnO)_3$ nanobelts was carried out in a horizontal tube furnace through a fully controlled chemical vapor deposition (CVD) process. Commercial ZnO and In and Ga powders were mixed, ground, and then loaded on an alumina boat and positioned at the center of the furnace, while Au-coated Si (100) substrates were placed downstream to collect the products. The furnace was heated to 1300 °C and held at this temperature for 10 min. During the whole growth, Ar was used as a carrier gas at a constant flow rate and pressure: 100 sccm and 50 Pa. After that, the furnace was naturally cooled down to room temperature.

The synthesized products were characterized by scanning electron microscopy (SEM, Hitachi, S4800), transmission electron microscopy (TEM, Philips CM 120), energy dispersive X-ray (EDX) spectrometry, selected area electron diffraction (SAED), and high-resolution transmission electron microscopy (HRTEM, Philips Tecnai 20). X-ray photoelectron spectra (XPS) were measured using an ESCALab220i-XL electron spectrometer (VG Scientific) using 300 W Al Kα radiation. The binding energies were referenced to the C-1s line at 284.6 eV of carbon. The FE properties were studied at room-temperature in a high vacuum chamber (2.6×10^{-6} Pa) using a 1 mm^2 cross-sectional area copper anode. A dc voltage sweeping from 100 to 1100 V was applied to the samples.

RESULTS AND DISCUSSION

Figure 1 shows a low magnification SEM image of a product, which reveals a large number of nanobelts covering the entire

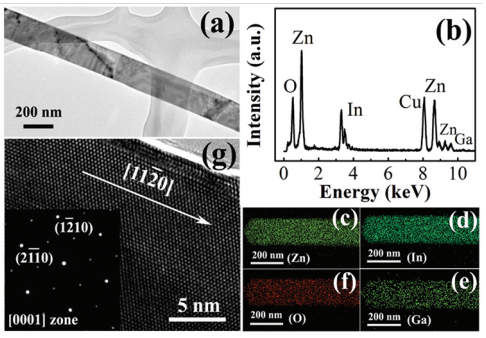

Figure 2. (a) Low-magnification TEM image; (b) EDX spectrum; (c−f) spatially resolved EDX elemental maps depicting the distribution of the constituting elements within the nanobelt: the images correspond to the Zn, In, Ga, and O signals, respectively; (g) HRTEM image projected along the *c*-axis of Ga-doped $In_2O_3(ZnO)_3$ nanobelts, where the inset represents the corresponding SAED pattern.

substrate. The nanobelts are several tens of micrometers in length. The detailed morphology and microstructure of the nanobelts are analyzed by TEM. A representative bright field TEM image of a single nanobelt is shown in Figure 2a. The nanobelt is thin and transparent, about 200 nm in width. The uneven contrast on the surface of the nanobelt indicates the presence of internal strain. From SEM and TEM results, there is no sign of any metal or alloy clusters at either ends of tens of nanobelts examined. Thus, the growth of the nanobelts does not follow the typical vapor−liquid−solid (VLS) growth mechanism, because an important feature of such mechanism is the existence of metal particles that are located at the growth fronts or roots and act as catalytic active sites. However, the Au particles play an important role and act as catalytically active sites during the formation of nanobelts in our experiment. Therefore, we suppose that the catalyst nanoparticles in our case may be buried under the nanobelts just like in case of the reported ZnSe nanowires[34] and $ZnGa_2O_4$ nanobelts.[35] The EDX microanalysis of a nanobelt is shown in Figure 2b. It illustrates that the nanobelt consists of In, Ga, Zn, and O. The Cu signal comes from the TEM sample grid. From quantitative EDX analyses, the atomic ratio of In/Ga/Zn is about 17:3.8:26, and the content of In and Ga (In + Ga/[Zn + In + Ga]) is estimated as 44 at. %. According to the phase diagram for the In_2O_3−ZnO system, the products here should crystallize into a $In_2O_3(ZnO)_3$ structure, in which some In atoms in the $InO^+(ZnO)_m$ block may be replaced by Ga atoms, forming the $In_{2-x}Ga_xO_3(ZnO)_3$ compound ($x \approx 0.37$).[36] Figure 2c−f shows the colored elemental maps of Zn, In, Ga, and O species, which give us an excellent visual grasp of spatially resolved elemental distribution. It is clearly seen that all elements are distributed uniformly within the whole nanobelt. The weaker contrast on the Ga map compared to those of Zn, In, and O confirms its status as a dopant. Figure 2g shows an HRTEM image taken perpendicular to the wide surface of a nanobelt along the [0001] zone axis. The resolved lattice fringes indicate that the nanobelt is single crystalline and its wide surface is parallel to the {0001} plane. The *d*-spacing between the two adjacent lattice fringes of {01$\bar{1}$0} planes of $In_2O_3(ZnO)_3$ is close to 0.29 nm and larger than 0.282 nm of ZnO. The growth of the nanobelt is along the <11$\bar{2}$0> direction. The corresponding SAED pattern is shown in the inset of Figure 2g. It should be noted that the intensity of the {11$\bar{2}$0} spots is obviously larger than that of the {01$\bar{1}$0} spots. This agrees well with the SAED pattern of

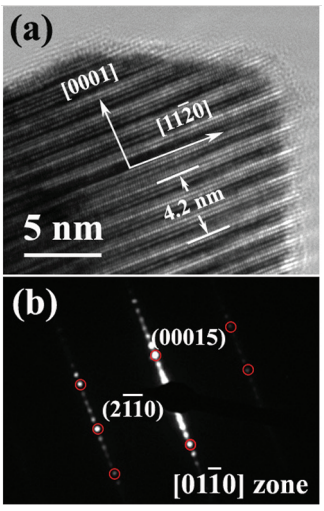

Figure 3. (a) HRTEM image projected along the [01$\bar{1}$0]of Ga-doped $In_2O_3(ZnO)_3$ nanobelts; (b) the corresponding SAED pattern.

$InGaO_3(ZnO)_3$ reported by Mader et al.[37] Similar results were obtained from tens of nanobelts.

The reason why we cannot observe the layered structure of $In_2O_3(ZnO)_3$ from the above TEM measurements is that the alternating layers of $In_2O_3(ZnO)_3$ stack along the [0001] direction, whereas the wide surface of the nanobelts is parallel to the {0001} plane. To observe the layered structure, TEM measurements should be performed in a direction perpendicular to the [0001] direction.[21] The HRTEM image taken from the lateral surface of a special narrow Ga-doped $In_2O_3(ZnO)_3$ nanobelt is shown in Figure 3a. It is along the <00$\bar{1}$0> zone axis, which is perpendicular to the [0001] direction. The superlattice periodicity is evident along the [0001] direction. It confirms the formation of the $In_2O_3(ZnO)_3$ superlattice structure. The lattice constant *c* equals to three times of the distance between the two adjacent InO_2^-layers and is about 4.2 nm.[24] That agrees well with the results reported by Moriga et al.[38] The corresponding SAED pattern is shown in Figure 3b. It consists of primary spots and four satellite spots along the *c*-axis between every two adjacent primary spots. The satellite diffraction spots are the typical feature during the formation of the $In_2O_3(ZnO)_3$ superlattice structure.

Further evidence of high crystal quality and desired compositions of the Ga-doped $In_2O_3(ZnO)_3$ nanobelts were obtained through XPS analysis. Figure 4a shows the survey spectrum of the Ga-doped $In_2O_3(ZnO)_3$ nanobelts. No peaks of other elements except Zn, In, Ga, O, and C are observed. The C peak comes from the atmospheric contamination due to air exposure. The binding energies obtained during the XPS analysis were corrected, taking into account the specimen charging and by referring to C-1s at 284.60 eV. High resolution XPS scans of Zn-2p, In-3d, and Ga-3d are shown in Figure 4b−d. The binding energies of the Zn-$2p_{3/2}$ and Zn-$2p_{1/2}$ peaks are located at 1022.2 and 1045.3 eV, respectively. The energy difference between the Zn-2p peaks is 23.1 eV (Figures 4d), which agrees well with the standard value of 22.97 eV.[28] The two peaks at 445.1 and 452.7 eV in Figure 4c correspond to the electronic states of $In3d_{3/2}$ and $In3d_{5/2}$, respectively. The energy difference between the In3d peaks is 7.6 eV; this agrees well with the standard value of 7.5 eV.[39] From the closer observation it is documented that the binding energies of

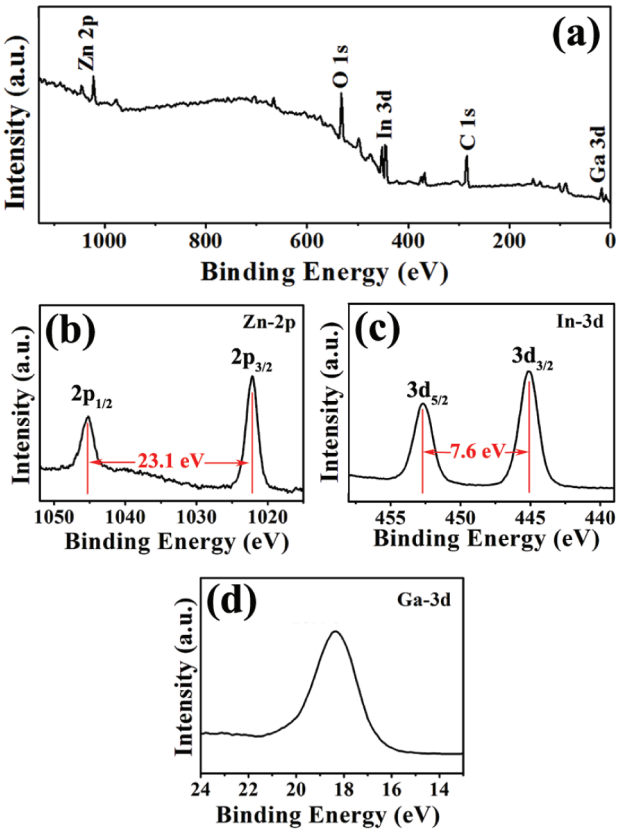

Figure 4. XPS analysis of the as-prepared Ga-doped $In_2O_3(ZnO)_3$ nanobelts: (a) survey spectrum; (b) Zn-2p binding energy spectrum; (c) In-3d binding energy spectrum; (d) Ga-3d binding energy spectrum.

Zn2p and In3d peaks both exhibit a positive shift in comparison to the standard values. This could be attributed to an electron transfer from Zn and In to Ga because of the stronger electronic interaction between Ga and O, as compared to Zn and In with O.[39,40] The peak of Ga-3d is located at 18.4 eV, as shown in Figure 4d. It reconfirms that Ga dopants are incorporated into the nanobelts and substitute In to form Ga−O bonds.

FE measurements show that the Ga-doped $In_2O_3(ZnO)_3$ nanobelts are valuable field emitters. Figure 5a illustrates the FE current density, *J*, as a function of the applied field, *E*, for a *J*−*E* plot at a working sample-anode distance of 200 μm. With the increase of the applied field *E*, the emission current density *J* has exponentially increased. The turn-on electric field is extrapolated as ~4.1 V/μm at a current density of 10 mA/cm^2. The low value of turn-on electric field surpass those mentioned in the previous reports on carbon nanotubes (5.2 V/μm),[41] ZnO (11 V/μm),[42] ZnS (5.43 V/μm),[43] CdS (12.2 V/μm),[4] and Si nanostructures (13 V/μm).[44] It suggests that the presently synthesized Ga-doped $In_2O_3(ZnO)_3$ nanobelts can be used as practical field emitters. The FE *J*−*E* characteristic is further analyzed by the Fowler−Nordheim (F−N) equation: $J = (A\beta^2E^2/\varphi)\exp(-B\varphi^{3/2}/\beta E)$ or $\ln(J/E^2) = \ln(A\beta^2/\varphi) - B\varphi^{3/2}/\beta E$, where *A* and *B* are constants ($A = 1.54 \times 10^{-6}$ A eV/V^2; $B = 6.83 \times 10^3$ V μm^{-1} eV$^{-3/2}$), *J* is the current density, β is the field-enhancement factor, *E* is the applied field, and φ is the work function of the emitting materials.[45,46] Here the assumed work function of $In_2O_3(ZnO)_3$, 5.3 eV, is the same as that of ZnO. Actually, it should be smaller than that because In and Ga doping would dramatically decrease

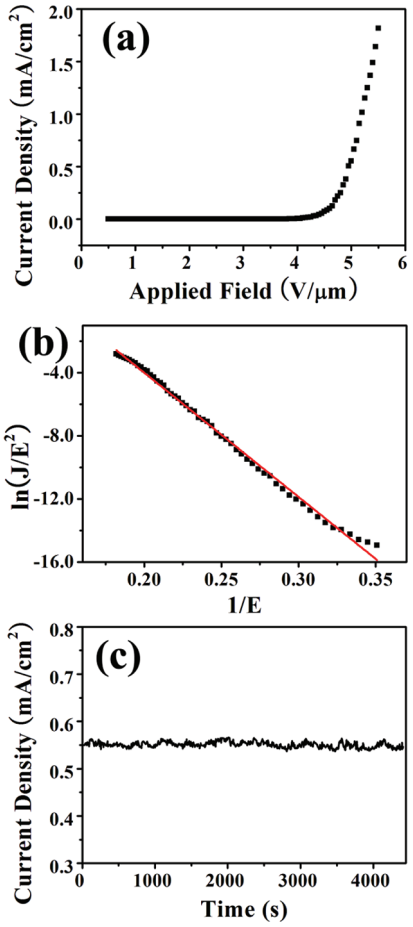

Figure 5. Field emission properties of Ga-doped $In_2O_3(ZnO)_3$ nanobelts: (a) FE current density versus the applied field ($J-E$) curve with a turn-on field of 4.1 V/μm at a current density of 10 mA/cm^2; (b) the corresponding Fowler−Nordheim (F−N) plot showing linear dependence; (c) the field-emission stability data acquired at the emission current density of 0.55 mA/cm^2.

the work function.[5,7,28−30] Figure 5b illustrates the variation of ln (J/E^2) with ($1/E$) for the Ga-doped $In_2O_3(ZnO)_3$ nanobelts. The plot fits well to a line given by the F−N equation within the measurement range. It demonstrates that FE from the Ga-doped In_2O_3-$(ZnO)_3$ nanobelts obeys the F−N behavior. Furthermore, the field enhancement factor calculated from the slope of the fitted straight line in Figure 5b is 1059. It is comparable to those mentioned in the previous reports on ZnO nanostructures.[7,28,30,47−49] The insignificant superiority of the Ga-doped $In_2O_3(ZnO)_3$ nanobelts in regards to the field enhancement factor may be due to looser alignments and particular dimensions (or aspect ratios). It is known that both alignments and dimensions have a significant influence on the emitter field-enhancement factor. It is reasonable to expect a higher field enhancement factor for the Ga-doped $In_2O_3(ZnO)_3$ nanostructures that have better alignments and sharper tips. The stability of field emitters is another important parameter related to potential applications. Figure 5c displays the stability of emission current density at an applied electric field of 5 V/μm over a period of 4500 s. There is no any current degradation or notable fluctuation during this period. The good emission stability demonstrated by the Ga-doped $In_2O_3(ZnO)_3$ nanobelts should be attributed to a good high-temperature stability of $In_2O_3(ZnO)_m$.

CONCLUSIONS

Ga-doped $In_2O_3(ZnO)_3$ nanobelts were successfully fabricated via a simple CVD process. These nanobelts demonstrate good FE performances. The turn-on electrical field is as low as 4.1 V/μm, and the field enhancement factor is 1059. The emission current density shows a good stability for 4500 s without any current degradation or notable fluctuation. The reported good FE performances are thought to be due to the layered superlattice structure of $In_2O_3(ZnO)_3$ and the effects of Ga doping.

AUTHOR INFORMATION

Corresponding Author

*E-mail: xtzhangzhang@hotmail.com; zhai.tianyou@gmail.com.

ACKNOWLEDGMENT

X.T.Z. would like to thank the support from the Natural Science Foundation of China (No. 51172058), the Key Project of Natural Science Foundation of Heilongjiang Province (ZD201112), and the Project of Overseas Talent, Personnel Bureau, Heilongjiang Province. (T.Y.Z.) thanks the International Center for Materials Nanoarchitectonics (MANA) of the National Institute for Materials Science (NIMS), Tsukuba, Japan.

REFERENCES

(1) Zhai, T. Y.; Li, L.; Ma, Y.; Liao, M. Y.; Wang, X.; Fang, X. S.; Yao, J. N.; Bando, Y.; Golberg, D. *Chem. Soc. Rev.* **2011**, *40*, 2986–3004.
(2) Gautam, U. K.; Panchakarla, L. S.; Dierre, B.; Fang, X. S.; Bando, Y.; Sekiguchi, T.; Govindaraj, A.; Golberg, D.; Rao, C. N. R. *Adv. Funct. Mater.* **2009**, *19*, 131–140.
(3) Fang, X. S.; Bando, Y.; Gautam, U. K.; Ye, C.; Golberg, D. *J. Mater. Chem.* **2008**, *18*, 509–522.
(4) Zhai, T. Y.; Fang, X. S.; Bando, Y. S.; Liao, Q.; Xu, X. J.; Zeng, H. B.; Ma, Y.; Yao, J. N.; Golberg, D. *ACS Nano* **2009**, *3*, 949–959.
(5) Karpyna, V. A.; Evtukh, A. A.; Semenenko, M. O.; Lazorenko, V. I.; Lashkarev, G. V.; Khranovskyy, V. D.; Yakimova, R.; Fedorchenko, D. A. *Microelectron. J.* **2009**, *40*, 229–231.
(6) Zhang, X. N.; Chen, Y. G.; Xie, Z. P.; Yang, W. Y. *J. Phys. Chem. C* **2010**, *114*, 8251–8255.
(7) Xu, C. X.; Sun, X. W.; Chen, B. J. *Appl. Phys. Lett.* **2004**, *84*, 1540–1542.
(8) Naghavi, N.; Marcel, C.; Dupont, L.; Rougier, A.; Leriche, J. B.; Guery, C. *J. Mater. Chem.* **2000**, *10*, 2315–2319.
(9) Masuda, Y.; Ohta, M.; Seo, W. S.; Pitschke, W.; Koumoto, K. *J. Solid State Chem.* **2000**, *150*, 221–227.
(10) Andrews, S. C.; Fardy, M. A.; Moore, M. C.; Aloni, S.; Zhang, M. J.; Radmilovic, V.; Yang, P. D. *Chem. Sci.* **2011**, *2*, 706–714.
(11) Wu, L. L.; Zhang, X. T.; Wang, Z. F.; Liang, Y.; Xu, H. Y. *J. Phys. D: Appl. Phys.* **2008**, *41*, 195406-1–5.
(12) Li, C. F.; Bando, Y.; Nakamura, M.; Kimizuka, N. *J. Electron Microsc.* **1997**, *46*, 119–127.
(13) Goncharuk, N. M. *Mater. Sci. Eng.* **2003**, *353*, 36–40.
(14) Wang, R. Z.; Ding, X. M.; Wang, B.; Xue, K.; Xu, J. B.; Yan, H.; Hou, X. Y. *Phys. Rev. B* **2005**, *72*, 125310-1–6.
(15) Wang, R. Z.; Yan, H.; Wang, B.; Zhang, X. W.; Hou, X. Y. *Appl. Phys. Lett.* **2008**, *92*, 142102-1–3.
(16) Zhao, W.; Wang, R. Z.; Song, X. M.; Wang, H.; Wang, B.; Yan, H.; Chu, P. K. *Appl. Phys. Lett.* **2011**, *98*, 152110-1–3.
(17) Zhao, W.; Wang, R. Z.; Han, S.; Xue, K.; Wang, H.; Yan, H. *J. Phys. Chem. C* **2010**, *114*, 11584–11587.
(18) Aleman, B.; Fernandez, P.; Piqueras, J. *Appl. Phys. Lett.* **2009**, *95*, 013111-1–3.

(19) Li, D. P.; Wang, G. Z.; Han, X. H. *J. Phys. D: Appl. Phys.* **2009**, *42*, 175308-1–5.
(20) Na, C. W.; Bae, S. Y.; Park, J. *J. Phys. Chem. B* **2005**, *109*, 12785–12790.
(21) Li, D. P.; Wang, G. Z.; Han, X. H.; Jie, J. S.; Lee, S. T. *J. Phys. Chem. C* **2009**, *113*, 5417–5421.
(22) Jie, J. S.; Wang, G. Z.; Han, X. H.; Hou, J. G. *J. Phys. Chem. B* **2004**, *108*, 17027–17031.
(23) Zhang, X. T.; Lu, H. Q.; Gao, H.; Wang, X. J.; Xu, H. Y.; Li, Q.; Hark, S. K. *Cryst. Growth Des.* **2009**, *9*, 364–367.
(24) Wu, L. L.; Liang, Y.; Liu, F. W.; Lu, H. Q.; Xu, H. Y.; Zhang, X. T.; Hark, S. K. *CrystEngComm* **2010**, *12*, 4152–4155.
(25) Niu, B. J.; Wu, L. L.; Zhang, X. T. *CrystEngComm* **2010**, *12*, 3305–3309.
(26) Nakamura, M.; Kimizuka, N.; Mohri, T. *J. Solid State Chem.* **1991**, *93*, 298–315.
(27) Ueda, Y.; Yoshida, K.; Saitoh, H. *J. Ceram. Soc. Jpn.* **2009**, *117*, 508–514.
(28) Chang, L. W.; Yeh, J. W.; Cheng, C. L.; Shieu, F. S.; Shih, H. C. *Appl. Surf. Sci.* **2011**, *257*, 3145–3151.
(29) Huang, Y. H.; Zhang, Y.; Gu, Y. S.; Bai, X. D.; Qi, J. J.; Liao, Q. L.; Liu, J. *J. Phys. Chem. C* **2007**, *111*, 9039–9043.
(30) Jung, M. N.; Ha, S. H.; Oh, S. J.; Koo, J. E.; Cho, Y. R.; Lee, H. C.; Lee, S. T.; Jeon, T. I.; Makino, H.; Chang, J. H. *Curr. Appl. Phys.* **2009**, *9*, E169–E172.
(31) Li, D. P.; Wang, G. Z.; Yang, Q. H.; Xie, X. *J. Phys. Chem. C* **2009**, *113*, 21512–21515.
(32) Wu, L. L.; Liu, F. W.; Chu, Z. Q.; Liang, Y.; Xu, H. Y.; Lu, H. Q.; Zhang, X. T.; Li, Q. A.; Hark, S. K. *CrystEngComm* **2010**, *12*, 2047–2050.
(33) Huang, D. L.; Wu, L. L.; Zhang, X. T. *J. Phys. Chem. C* **2010**, *114*, 11783–11786.
(34) Zhang, X. T.; Liu, Z.; Leung, Y. P.; Li, Q.; Hark, S. K. *Appl. Phys. Lett.* **2003**, *83*, 5533-1–3.
(35) Wu, L. L.; Zhang, X. T.; Liang, Y.; Xu, H. Y. *J. Alloys Compd.* **2009**, *468*, 452–454.
(36) Moriga, T.; Edwards, D. D.; Mason, T. O.; Palmer, G. B.; Poeppelmeier, K. R.; Schindler, J. L.; Kannewurf, C. R.; Nakabayashi, I. *J. Am. Ceram. Soc.* **1998**, *81*, 1310–1316.
(37) Keller, I.; Assenmacher, W.; Schnakenburg, G.; Mader, W. *Z. Anorg. Allg. Chem.* **2009**, *635*, 2065–2071.
(38) Moriga, T.; Kammler, D. R.; Mason, T. O.; Palmer, G. B.; Poeppelmeier, K. R. *J. Am. Ceram. Soc.* **1999**, *82*, 2705–2710.
(39) Ahmad, M.; Sun, H. Y.; Zhu, J. *ACS Appl. Mater. Interfaces* **2011**, *3*, 1299–1305.
(40) Kim, G. H.; Jeong, W. H.; Kim, H. J. *Phys. Status Solidi A* **2010**, *207*, 1677–1679.
(41) Li, C.; Zhang, Y.; Mann, M.; Hiralal, P.; Unalan, H. E.; Lei, W.; Wang, B. P.; Chu, D. P.; Pribat, D.; Amaratunga, G. A. J.; et al. *Appl. Phys. Lett.* **2010**, *96*, 143114-1–3.
(42) Lee, C. J.; Lee, T. J.; Lyu, S. C.; Zhang, Y.; Ruh, H.; Lee, H. J. *Appl. Phys. Lett.* **2002**, *81*, 3648-1–3.
(43) Gautam, U. K.; Fang, X. S.; Bando, Y.; Zhan, J. H.; Golberg, D. *ACS Nano* **2008**, *2*, 1015–1021.
(44) Shang, N. G.; Meng, F. Y.; Au, F. C. K.; Li, Q.; Lee, C. S.; Bello, I.; Lee, S. T. *Adv. Mater.* **2002**, *14*, 1308–1313.
(45) Li, L.; Fang, X. S.; Chew, H. G.; Zheng, F.; Liew, T. H.; Xu, X. J.; Zhang, Y. X.; Pan, S. S.; Li, G. H.; Zhang, L. D. *Adv. Funct. Mater.* **2008**, *18*, 1080–1088.
(46) Zhai, T. Y.; Fang, X. S.; Bando, Y.; Dierre, B.; Liu, B. D.; Zeng, H. B.; Xu, X. J.; Huang, Y.; Yuan, X. L.; Sekiguchi, T.; et al. *Adv. Funct. Mater.* **2009**, *19*, 2423–2430.
(47) Huang, X. X.; Cheng, C. L.; Chen, Y. T.; Chen, Y. F. *J. Appl. Phys.* **2010**, *108*, 063717-1–4.
(48) Pan, H.; Zhu, Y. W.; Sun, H.; Feng, Y. P.; Sow, C. H.; Lin, J. Y. *Nanotechnology* **2006**, *17*, 5096–5100.
(49) Xue, X. Y.; Li, L. M.; Yu, H. C.; Chen, Y. J.; Wang, Y. G.; Wang, T. H. *Appl. Phys. Lett.* **2006**, *89*, 043118-1–3.